Journal of Bacteriology

| Bacteriology | Full-Length Text

# The *hiuABC* operon mediates xenosiderophore utilization in *Caulobacter crescentus*

**Sergio Hernandez-Ortiz,**[1] **Aretha Fiebig,**[1] **Sean Crosson**[1]

**AUTHOR AFFILIATION** See affiliation list on p. 13.

**ABSTRACT** *Caulobacter* species are common residents of soil and aquatic ecosystems, where bioavailable iron is often extremely limited. Like other diderm bacteria, *Caulobacter crescentus* can acquire Fe(III) via outer-membrane TonB-dependent transporters (TBDTs) that recognize and import ferric siderophore complexes. Although *C. crescentus* is not known to synthesize siderophores, it encodes multiple TBDTs that are transcriptionally regulated by the ferric uptake repressor (Fur), suggesting it acquires iron by scavenging xenosiderophores produced by neighboring microbes. To identify *C. crescentus* genes required for xenosiderophore utilization, we developed a barcoded transposon screen using ferrioxamine B (FXB), a hydroxamate-family siderophore produced by soil actinomycetes, as a model substrate. This screen identified *hiuABC*, a conserved, Fur-regulated operon that supports FXB-dependent iron acquisition. We provide evidence that *hiuA* encodes the primary TBDT responsible for uptake of ferrioxamines and ferrichrome (FC), structurally distinct members of the hydroxamate siderophore family. *hiuB* encodes a PepSY-domain protein with structural similarity to *Pseudomonas aeruginosa* FoxB, a known periplasmic ferri-siderophore reductase. *hiuC* encodes a small, hypothetical membrane protein predicted to form a functional complex with HiuB in the inner membrane. Both *hiuB* and *hiuC* are required for utilization of FXB and ferrioxamine E, indicating a shared role in iron acquisition from ferrioxamines. Surprisingly, utilization of FC as an iron source required *hiuB* but not *hiuC*, suggesting a substrate-specific role for HiuC in ferri-siderophore processing. We conclude that the conserved *hiuABC* operon encodes a set of proteins that enable bacteria to acquire iron from structurally diverse hydroxamate-family siderophores.

**IMPORTANCE** Iron is often a limiting nutrient due to its poor solubility in the presence of oxygen. To overcome this, some microbes produce specialized molecules known as siderophores, which tightly bind and solubilize iron, facilitating its uptake into the cell. *Caulobacter* species are common in freshwater, marine, and soil environments, and there is emerging evidence that they play important roles in plant-associated microbial communities. Here, we report the discovery of a three-gene system that allows *Caulobacter crescentus* to acquire iron from a set of siderophores produced by select soil bacteria and fungi. We define functional roles for each protein component of this system, which informs a mechanism by which *Caulobacter* can pirate iron-scavenging molecules produced by its neighbors.

**KEYWORDS** siderophore, ferrioxamine, ferrichrome, hydroxamate, iron, PepSY domain, TnSeq, FoxB, TonB-dependent transporter, Fur

Iron is an essential nutrient required by nearly all organisms, serving as a cofactor in key biological processes including cellular respiration, DNA repair, and gas sensing (1). Though it is among the most abundant elements in the Earth's crust (2), iron is often a limiting nutrient in oxygenated environments because ferric iron (Fe[III]) forms insoluble

**Editor** Tao Dong, Southern University of Science and Technology, Shenzhen, Guangdong, China

Address correspondence to Sean Crosson, crosson4@msu.edu.

The authors declare no conflict of interest.

See the funding table on p. 13.

**Received** 5 September 2025
**Accepted** 22 December 2025
**Published** 4 February 2026

Copyright © 2026 Hernandez-Ortiz et al. This is an open-access article distributed under the terms of the Creative Commons Attribution 4.0 International license.

hydroxides and oxides at neutral pH (3). The concentration of bioavailable Fe(III) in aerobic soils and waters can be as low as $10^{-18}$ M at pH 7, far below the concentration needed to support microbial growth (4). In these conditions, microbes often obtain iron from their surroundings through the secretion of siderophores, which are high-affinity Fe(III)-chelating molecules that solubilize iron from minerals or organic complexes (5). More than 500 siderophores have been identified across diverse ecological niches (6, 7).

Diderm bacteria face an additional challenge in iron acquisition due to their double-membrane cell envelope. Siderophores and other organic iron complexes are often too large or too dilute to rely on passive diffusion across the cell envelope. To actively acquire iron, diderms employ TonB-dependent transporters (TBDTs), which are specialized outer membrane β-barrel receptors that bind and transport many substrates, including ferric-siderophore complexes (8). TBDTs exhibit specificity for particular structural classes of siderophores (e.g., catecholates, hydroxamates, or hydroxy-carboxylates) (9). Upon siderophore binding, the TBDT undergoes structural changes that expose its TonB box, enabling engagement with the TonB protein, which is anchored in the inner membrane. TonB is energized by proton motive force from the ExbB–ExbD complex and drives the structural rearrangements that enable import of the ferri-siderophore through the TBDT and into the periplasm (8). Once in the periplasm, ferri-siderophores may either be reduced locally or delivered to an ABC transporter for translocation into the cytoplasm (10).

*Caulobacter* species are metabolically versatile (11–16) aerobic diderms that are common in terrestrial and aquatic ecosystems (17) and have been identified as hub species in plant microbial communities (18, 19). The well-studied model system, *Caulobacter crescentus*, lacks known siderophore biosynthesis genes, but it encodes 62 predicted TBDTs. It is therefore likely that this bacterium has the capacity to recognize and import a diverse array of siderophores produced by other microorganisms (i.e., xenosiderophores) (20–22). Indeed, iron limitation is known to de-repress transcription of four Fur-regulated TBDT genes in *C. crescentus: cciT*, CCNA_00138, *hutA*, and CCNA_03023 (23). While *hutA* encodes a characterized heme/hemin transporter (20), the substrates for *cciT*, CCNA_00138, and CCNA_03023 (hereafter referred to as *hiuA*) remain undefined.

Hydroxamate siderophores, including the linear trihydroxamate ferrioxamine B (FXB) and the cyclic hexapeptide ferrichrome (FC), are common in terrestrial ecosystems (7) and promote *C. crescentus* growth under iron-limiting conditions (20), but the specific TBDTs mediating their uptake remain unidentified. Furthermore, the fate of ferric–siderophore complexes in the periplasm is poorly characterized in this important model bacterium. To address these knowledge gaps, we developed a broth-based genetic screening platform for analyzing siderophore acquisition mechanisms in *C. crescentus*. Here, we report a genome-wide approach to identify hydroxamate siderophore acquisition genes in *C. crescentus* using a barcoded transposon mutant library. Building on prior work showing that EDTA treatment of complex medium induces iron starvation and that ferri-siderophore supplementation restores growth (24), we used FXB as a model exogenous iron source in our screen. Our approach uncovered a Fur-regulated three-gene *h*ydroxamate *i*ron *u*ptake operon (*hiuA*, *hiuB*, and *hiuC*) that supports utilization of structurally distinct hydroxamate-type ferri-siderophores that are common in soil and aquatic environments. This manuscript describes functional and structural analyses of the products of the *hiu* operon.

## RESULTS

### Desferrioxamine limits intracellular iron and restricts *Caulobacter* growth, while FXB enhances growth under iron-limiting conditions

We began by testing whether 1 µM desferrioxamine B, the iron-free form of FXB, inhibits the growth of wild-type (WT) *C. crescentus* in a peptone yeast extract (PYE) complex broth. Desferrioxamine B binds Fe(III) with exceptionally high affinity (25) and thus will chelate and potentially sequester iron present in the growth medium. We compared growth in the presence of 1 µM desferrioxamine B to that in 300 µM

EDTA, a well-characterized cation chelator known to limit *C. crescentus* growth by reducing intracellular iron availability (24). The PYE broth produced in our laboratory contains approximately 700 nM iron (24), so the concentration of desferrioxamine used in this experiment exceeded available iron in the medium. Growth yield of *C. crescentus* cultures, measured by $OD_{660}$, was reduced in the presence of desferrioxamine B compared to growth in plain PYE or PYE supplemented with 300 µM EDTA (Fig. 1A). This suggested that (i) desferrioxamine B is a more potent inhibitor of *C. crescentus* growth than EDTA, and (ii) the iron-loaded form of the siderophore, FXB, is not efficiently imported at the tested concentration.

We predicted that growth inhibition by desferrioxamine B was associated with intracellular iron limitation. To test this, we measured transcription from four Fur-regulated promoters ($P_{feoAB}$, $P_{cciT}$, $P_{hutA}$, and $P_{CCNA_03023}$) fused to a fluorescent reporter gene, mNeonGreen. Transcription from these Fur-regulated promoters was significantly higher in media containing 1 µM desferrioxamine B compared to untreated medium (Fig. 1B), providing evidence that this concentration of desferrioxamine B reduces available iron in the cytoplasm and thus attenuates *C. crescentus* growth via iron limitation. Furthermore, each promoter exhibited significantly higher activity in the presence of 1 µM desferrioxamine B compared to 300 µM EDTA, indicating that 1 µM desferrioxamine B imposes a stronger iron limitation than 300 µM EDTA.

Finally, we tested whether the addition of 1 µM FXB (the iron-bound form of desferrioxamine B) to EDTA-treated growth medium mitigated the growth-limiting effect of 300 µM EDTA. FXB binds Fe(III) with an affinity 5–6 orders of magnitude greater than that of EDTA and is therefore expected to retain Fe(III) even in the presence of a 300-fold molar excess of EDTA (25). Growth of the WT strain was significantly improved with FXB supplementation relative to broth containing EDTA only, though the effect was modest (Fig. S1). Evidence that this growth enhancement effect is due to the acquisition of iron from FXB is presented below.

## A role for the CCNA_03023-21 operon (*hiuABC*) in iron acquisition from FXB

Our observation that 1 µM of the ferri-siderophore FXB enhanced growth under EDTA-mediated iron limitation (Fig. S1) prompted us to investigate the genetic basis of FXB-dependent iron acquisition. To do so, we employed Randomly Barcoded Transposon Sequencing (RB-TnSeq) (26) cultivating a *C. crescentus* transposon mutant library (27, 28)

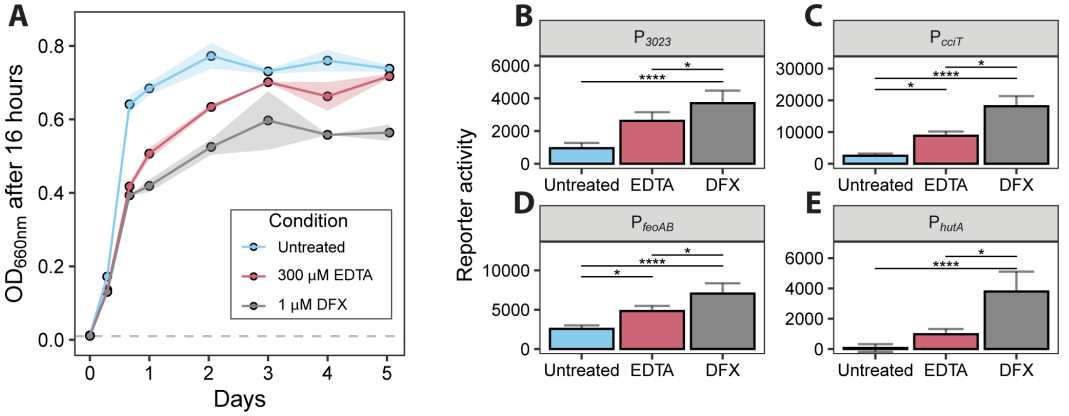



**FIG 1** Growth inhibition by desferrioxamine is associated with reduced intracellular iron. (A) Optical density ($OD_{660}$) of *C. crescentus* CB15 cultures grown in PYE broth for 5 days with or without 300 µM EDTA or 1 µM desferrioxamine B (DFX). Cultures were inoculated at an initial $OD_{660}$ of 0.01 (dashed gray line). Values represent the mean ± SD (shaded areas) of six cultures grown in two independent experiments. (B–E) Fluorescence reporter assays measuring transcription from Fur-regulated promoters: (B) CCNA_03023 ($P_{3023}$), (C) *cciT* ($P_{cciT}$), (D) *feoAB* ($P_{feoAB}$), and (E) *hutA* ($P_{hutA}$). Strains carrying promoter fusions to the mNeonGreen fluorescent protein were grown for 2 h in PYE broth with or without 300 µM EDTA or 1 µM desferrioxamine. Bar plots show average fluorescence normalized to $OD_{660}$, with error bars representing one standard deviation ($n = 9$). Statistical comparisons were performed using a Kruskal–Wallis test followed by Dunn's post-test. Significance: * $P < 0.05$; **** $P < 0.0001$.

in PYE broth supplemented with 300 µM EDTA, with or without 1 µM FXB. FXB conferred only a modest growth rescue in EDTA-treated broth, so we serially passaged cultures in this experiment to amplify fitness defects (and possibly, advantages) associated with specific transposon insertions. This approach yielded mutant strains that appeared to be defective in iron acquisition from FXB (Fig. 2; Table S1).

Inspection of mutant fitness scores revealed distinct mutant categories (Fig. 2A; Fig. S2). As expected from previous studies, most mutants showed no detectable fitness difference in any treatment condition, whereas others were similarly fitness impaired in both EDTA-treated and EDTA + FXB-supplemented media. We also observed several notable fitness patterns across treatments (Fig. S2). In untreated PYE, mutants defective in holdfast synthesis and attachment showed higher apparent fitness because they remain enriched in the bulk culture rather than adhering to the culture well walls as previously described (28). This effect was amplified in EDTA and partially reversed when FXB was added, suggesting a connection between holdfast-mediated surface adherence and iron availability. Disruption of select heme and hemoprotein biosynthesis genes resulted in modest fitness defects in untreated media, had no effect in EDTA, and conferred a slight fitness advantage in EDTA supplemented with FXB. In contrast, disruption of select sphingolipid biosynthesis genes (29–31) caused fitness defects under all three conditions, with only minor attenuation upon addition of FXB to EDTA. The most striking mutants in the screen were those with fitness defects specifically in the FXB-supplemented condition but not in EDTA alone, including strains with insertions in *CCNA_00973* (protein tyrosine phosphatase), *CCNA_03022* (PepSY-family inner

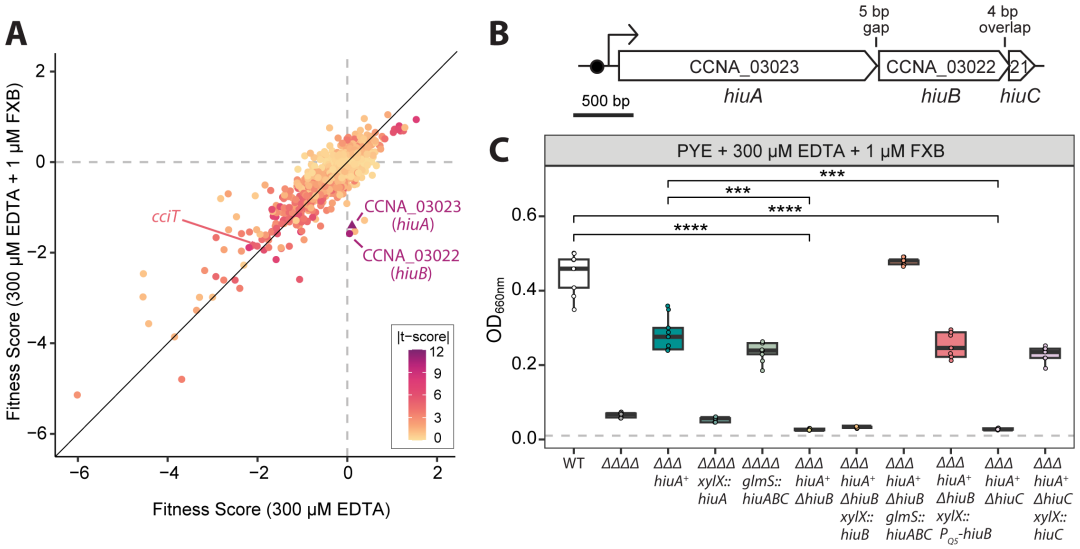



**FIG 2** Genetic screen identifies genes in the *hiu* operon that support *C. crescentus* fitness during growth on FXB as the sole iron source. (A) Gene fitness scores derived from a genome-wide screen using a barcoded *C. crescentus* Tn-himar mutant library after growth in complex PYE medium supplemented with 300 µM EDTA (iron-depleted condition) or with 300 µM EDTA plus 1 µM FXB. Each point represents the mean fitness score for a single gene, averaged across four independent cultures per condition. Dot color reflects the *t*-score associated with each fitness value, providing a measure of statistical confidence in the fitness effect. The *cciT,* CCNA_00138, *hutA,* and *hiuA* are represented by the following shapes, respectively: diamond, square, downward triangle, and upward triangle. Both CCNA_00138 and *hutA* are hidden by the mass of dots. Genes required specifically for growth in the presence of FXB exhibit no fitness defects in the presence of only EDTA but negative fitness scores when grown with FXB. Complete fitness scores are provided in Table S1. (B) Diagram of the *hiuA–hiuB–hiuC* locus (*CCNA_03023–03021*). A predicted Fur-binding site (Fur box) upstream of the locus is indicated by a black circle. (C) Optical density ($OD_{660}$) measurements of *C. crescentus* strains grown for 16 h in PYE broth supplemented with 300 µM EDTA and 1 µM FXB. Strains are WT, lacking all four fur-regulated TBDTs including *hiuA* (ΔΔΔΔ), lacking three fur-regulated TBDTs and encoding only *hiuA* (*hiuA*$^+$ΔΔΔ), and derived strains lacking either *hiuB* or *hiuC* and/or carrying ectopic expression constructs for *hiuA*, *hiuB*, *or hiuC*. Full strain genotypes can be found in Table S2. Cultures were inoculated at an initial $OD_{660}$ of 0.01 (dashed gray line) and grown for 16 h. Box plots show the median and interquartile range (25th–75th percentiles), overlaid with individual replicate values ($n = 9$). Comparisons of $OD_{660}$ between strains were performed using a Kruskal-Wallis test followed by Dunn's post-test. Statistical significance is indicated as follows: ***$P < 0.001$ and ****$P < 0.0001$.

membrane protein), *CCNA_03023* (TonB-dependent outer membrane transporter, TBDT), and *CCNA_03277* (glycosyltransferase).

To prioritize candidates for further analysis, we inspected the *t*-scores associated with mutant fitness values under FXB-supplemented conditions. The *t*-score reflects the statistical confidence of fitness values for particular genes (26). CCNA_03022 and CCNA_03023 mutants had the highest *t*-scores ($t > |10|$), indicating that strains harboring insertions in these genes had consistent and significant growth defects in this condition. CCNA_03023 encodes a TBDT related to *Escherichia coli* FhuA (20), a transporter known to mediate the uptake of ferric hydroxamate siderophores (32). CCNA_03022 encodes a predicted inner membrane protein of the PepSY-PiuB superfamily (33). These two genes, along with CCNA_03021 (encoding a predicted 61-residue hypothetical inner membrane protein), comprise an operon that is regulated by Fur, as evidenced by published transcriptomic analyses and global transcription start site mapping (23, 34) (Fig. 2B). CCNA_03021 was not identified in our RB-TnSeq screen as it contains only a single TnHimar (i.e., TA dinucleotide) insertion site, though this gene is syntenic with CCNA_03022 and CCNA_03023 across Proteobacteria and in Bacteroidota (Fig. S3), suggesting it shares a functional role in iron acquisition from FXB. We hereafter refer to these genes as hydroxamate iron uptake A through C: *hiuA* (gene locus CCNA_03023), *hiuB* (gene locus CCNA_03022), and *hiuC* (gene locus CCNA_03021).

## HiuA is the primary TBDT for FXB uptake, and its function requires HiuB and HiuC

To test whether *hiuA* encodes the primary TBDT for FXB uptake, we used a set of strains in which three of the four Fur-regulated TBDTs have been deleted (denoted ΔΔΔ). Each strain retained only one of the four Fur-regulated outer membrane transporters: HiuA (ΔΔΔ *hiuA*$^+$), CciT (ΔΔΔ *cciT*$^+$), CCNA_00138 (ΔΔΔ *138*$^+$), or HutA (ΔΔΔ *hutA*$^+$). In PYE medium containing 300 µM EDTA, growth was abolished in all strains except ΔΔΔ *cciT*$^+$ (Fig. S4). Addition of 1 µM FXB had only a marginal effect (~10% increase) on the growth of both WT and ΔΔΔ *cciT*$^+$ strains (Fig. S5). The ΔΔΔ *138*$^+$ and ΔΔΔ *hutA*$^+$ strains remained growth defective in the presence of EDTA but showed slight FXB-dependent growth enhancement. In contrast, the ΔΔΔ *hiuA*$^+$ strain exhibited a ~200% increase in growth upon 1 µM FXB addition (Fig. S5). These results indicate that HiuA is the primary outer membrane transporter responsible for FXB uptake in *C. crescentus*.

To dissect the roles of other genes in the *hiuABC* operon, we constructed in-frame deletions of *hiuB* and *hiuC* in the ΔΔΔ *hiuA*$^+$ background, generating the ΔΔΔ *hiuA*$^+$ Δ*hiuB* and ΔΔΔ *hiuA*$^+$ Δ*hiuC* strains. A strain lacking all four Fur-regulated TBDTs (ΔΔΔΔ) served as a negative control. When grown in EDTA- and FXB-supplemented medium, the ΔΔΔ *hiuA*$^+$ strain again exhibited robust FXB-stimulated growth, while the ΔΔΔΔ, ΔΔΔ *hiuA*$^+$ Δ*hiuB*, and ΔΔΔ *hiuA*$^+$ Δ*hiuC* strains failed to respond to FXB (Fig. 2C). Ectopic expression of *hiuC* alone (driven by fusion to the native *hiuABC* operonic promoter) restored FXB-dependent growth in the ΔΔΔ *hiuA*$^+$ *ΔhiuC* strain, but ectopic expression of *hiuA* or *hiuB* individually from the operonic promoter did not restore growth in corresponding deletion strains in the presence of FXB (ΔΔΔΔ and ΔΔΔ *hiuA*$^+$ Δ*hiuB*, respectively; Fig. 2C). However, the expression of the full *hiuABC* operon successfully rescued the growth defects of both ΔΔΔΔ and ΔΔΔ *hiuA*$^+$ *ΔhiuB* strains in FXB (Fig. 2C). It is notable that complementation of ΔΔΔ *hiuA*$^+$ *ΔhiuB* with the full *hiuABC* operon restored growth to WT levels, which is higher than the parent *hiuA*$^+$ background; this is discussed below.

We further constructed a cumate-inducible expression system (35) for *hiuB* (pPTM057-PQ5-*hiuB*). In contrast to our construct in which *hiuB* was fused directly to the operonic promoter, expression of *hiuB* from the plasmid pPTM057-PQ5 successfully restored FXB-dependent growth in the *hiuA*$^+$ *ΔhiuB* strain to levels comparable to those of the ΔΔΔ *hiuA*$^+$ parent (Fig. 2C; Fig. S6). This result implies that artificially driven expression of *hiuB* from the operonic promoter (from a single chromosomal site) is insufficient for complementation, potentially due to suboptimal expression levels. The enhanced growth observed upon expression of the full *hiuABC* operon in the *hiuA*$^+$ Δ*hiuB*

background (Fig. 2C) likely reflects the presence of an additional copy of *hiuA* in this strain; HiuA levels may thus limit growth in the presence of a non-optimal substrate like FXB.

To contextualize these complementation results, prior studies have identified two antisense RNAs originating within the *hiuA* coding region (34, 36), suggesting that the *hiuABC* operon is subject to post-transcriptional regulation. Supporting this, ribosome profiling has revealed marked differences in the translational efficiencies of *hiuA*, *hiuB*, and *hiuC* (37), indicating complex post-transcriptional control that may substantially affect expression levels and may be disrupted in single-gene promoter fusion constructs. Taken together, our results provide evidence that the HiuABC system serves as the primary FXB transporter in *C. crescentus*, and acquisition of iron from FXB (transported via HiuA) requires the inner membrane proteins, HiuB and HiuC. Distinct genetic complementation results were observed when we used a higher-affinity HiuA substrate (FC) and are presented in a section below.

## The inner membrane proteins HiuB and HiuC support FXB utilization independently of the outer membrane import route

The ΔΔΔΔ strain lacks all four Fur-regulated TBDTs (including HiuA) but exhibited a slight growth enhancement when supplemented with 1 µM FXB (Fig. 3), suggesting the existence of alternative, lower-affinity FXB acquisition mechanisms. To test this, we cultured WT, ΔΔΔ *hiuA*$^+$, and ΔΔΔΔ strains in PYE + 300 µM EDTA that was supplemented with increasing concentrations of FXB (1–10 µM). FXB enhanced growth in all strains in a concentration-dependent manner, with the *hiuA*$^+$ strain reaching WT-like levels of growth at 3 µM FXB (Fig. 3A). Growth of the ΔΔΔΔ strain was impaired relative to WT, as expected, but was still enhanced by increasing FXB. We conclude that Fe(III) from FXB can be acquired via mechanisms that do not require any of the four known Fur-regulated TBDTs.

To test whether the inner membrane proteins HiuB and HiuC function specifically with the outer membrane transporter HiuA or are more broadly required for FXB utilization, we measured the growth of ΔΔΔ *hiuA*$^+$ *or* ΔΔΔΔ strains in which Δ*hiuB* or Δ*hiuC* was deleted in PYE + 300 µM EDTA supplemented with 10 µM FXB (i.e., the concentration that produced the greatest growth enhancement in the ΔΔΔΔ strain). Neither ΔΔΔ *hiuA*$^+$ *ΔhiuB* nor ΔΔΔ *hiuA*$^+$ *ΔhiuC* grew under these conditions (Fig. 3B). Similarly, deleting either *hiuB* or *hiuC* in the ΔΔΔΔ background eliminated the FXB-dependent growth enhancement observed at high FXB concentrations. We conclude that *hiuA* provides the most efficient route of FXB import across the outer membrane, but *hiuB* and *hiuC* are required to process the iron from FXB regardless of the outer membrane entry route.

## The *hiuABC* operon supports iron acquisition from ferrioxamine E

Since the *hiuABC* operon supports FXB-dependent growth enhancement during EDTA chelation challenge, we tested whether it also supports iron acquisition from the related (but structurally distinct) cyclic trihydroxamate siderophore, ferrioxamine E (FXE). Supplementation of PYE broth + 300 µM EDTA with 1 µM FXE did not increase culture density after 16 h (Fig. S7), which indicated that *C. crescentus* either lacks an efficient uptake mechanism for FXE or simply cannot acquire iron from FXE.

To distinguish between these possibilities, we increased the FXE concentration to 10 µM. The ΔΔΔΔ strain lacking all four Fur-regulated TBDTs showed a modest growth improvement at 10 µM FXE, while the ΔΔΔ *hiuA*$^+$ strain exhibited a more pronounced growth rescue (Fig. S7). As with FXB, FXE-dependent growth enhancement required both *hiuB* and *hiuC*. These results indicate that iron acquisition from FXE, although less efficient than FXB, also proceeds through mechanisms that require the HiuB and HiuC inner membrane proteins.

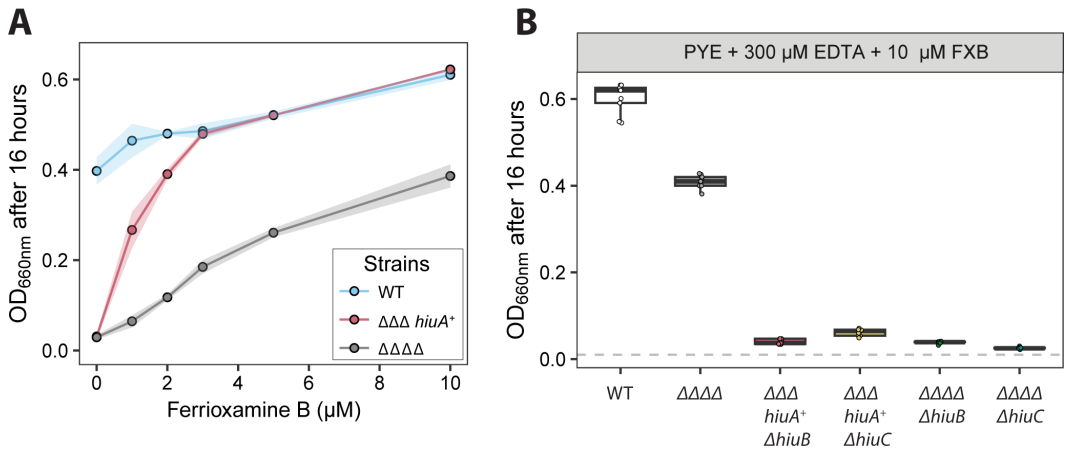



**FIG 3** Utilization of FXB requires *hiuA*, *hiuB*, and *hiuC*. (A) Growth ($OD_{660}$) of WT, ΔΔΔ *hiuA*$^+$, and the ΔΔΔΔ strain (lacking all four fur-regulated TBDTs, including *hiuA*), grown for 16 h in PYE medium containing 300 µM EDTA and increasing concentrations of FXB. Each point represents the mean, and shaded areas represent the standard deviation of nine biological replicates performed on separate days. (B) Endpoint $OD_{660}$ values of WT, ΔΔΔΔ, and mutants lacking *hiuB* or *hiuC* in the ΔΔΔ *hiuA*$^+$ and ΔΔΔΔ backgrounds cultures after 16 h of growth in PYE with 300 µM EDTA and 10 µM FXB. Box plots show the median and interquartile range (25th–75th percentiles), overlaid with individual data points ($n$ = 9). Cultures were inoculated at $OD_{660}$ = 0.01 (dashed gray line).

## HiuA and HiuB, but not HiuC, are required for FC utilization

Thus far, we have presented evidence that the *hiuABC* operon facilitates iron acquisition from the structurally related trihydroxamate siderophores FXB and FXE. To test whether *hiuABC* supports utilization of a hydroxamate siderophore belonging to another structural class, we measured *C. crescentus* growth in PYE medium containing 300 µM EDTA supplemented with 1 µM FC, a cyclic hexapeptide hydroxamate.

Growth of the ΔΔΔΔ strain, which lacks all four Fur-regulated TBDTs, was only weakly enhanced by FC, suggesting minimal acquisition of iron from FC in this background (Fig. 4 and 5). In contrast, the strain encoding only *hiuA* (ΔΔΔ *hiuA*$^+$) exhibited WT levels of growth in the presence of 1 µM FC, indicating that HiuA enables efficient import of FC. Deletion of *hiuB* in this background (ΔΔΔ *hiuA*$^+$ *ΔhiuB*) abolished the growth enhancement conferred by FC, while deletion of *hiuC* (ΔΔΔ *hiuA*$^+$ *ΔhiuC*) had no effect (Fig. 4). These results support a model in which HiuB is necessary for iron acquisition from FC transported through the HiuA outer membrane receptor, while HiuC is not. Genetic complementation of *hiuA*$^+$ *ΔhiuB* with *hiuB* that was ectopically expressed from the operonic promoter restored FC-dependent growth, as did expression of the full *hiuABC* operon. Similarly, ectopic expression of *hiuA* from the operonic promoter in the ΔΔΔΔ background was sufficient to restore FC-dependent growth, confirming a role for *hiuA* and *hiuB* in FC utilization.

We next compared FC-dependent growth enhancement across strains encoding single Fur-regulated TBDTs. As previously shown, *cciT* confers WT-like growth in the presence of EDTA (24), while *hiuA* alone enabled WT growth in the presence of 1 µM FC and uniquely supported growth at FC concentrations as low as 100 nM (Fig. 5). In contrast, strains encoding only *CCNA_00138* or *hutA* exhibited only modest growth at 1 µM FC and failed to grow appreciably at lower FC levels (Fig. 5B). These results indicate that HiuA functions as a high-affinity FC transporter and suggest that it is the only Fur-regulated TBDT capable of supporting efficient iron acquisition from this cyclic peptide hydroxamate at low FC concentrations. We conclude that acquisition of iron from low-concentration FC requires both HiuA and HiuB, but not HiuC.

## The *hiuABC* operon does not support aerobactin utilization

Given that HiuA functions as a high-affinity receptor for ferrioxamines (FXB and FXE) and FC, we next asked whether the HiuABC system supports utilization of aerobactin

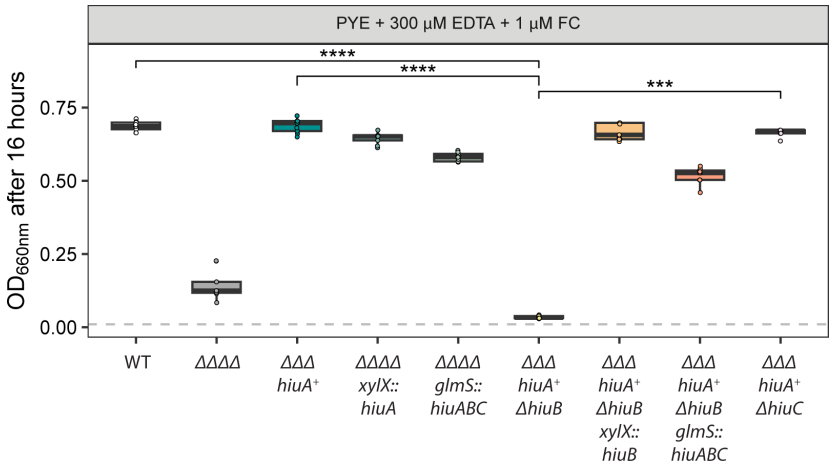



**FIG 4** HiuA and HiuB support *C. crescentus* growth on ferrichrome (FC). Optical density ($OD_{660}$) measurements of *C. crescentus* strains grown for 16 h in PYE broth supplemented with 300 µM EDTA and 1 µM FC. Strains include WT, ΔΔΔΔ (lacking all four Fur-regulated TBDTs), *hiuA*$^+$ΔΔΔ (encoding only *hiuA*), strains derived from *hiuA*$^+$ΔΔΔ with additional deletions in either *hiuB* or *hiuC*, and strains complemented with the respective deleted genes. Box plots show the median, 25th, and 75th percentiles, overlaid with individual data points from each independent culture ($n = 9$). Statistical comparisons of $OD_{660}$ between strains were performed using a Kruskal–Wallis test followed by Dunn's post test. Significance is indicated as: ***$P < 0.001$ and ****$P < 0.0001$.

(AB), a citrate-bis-hydroxamate siderophore. Unlike FXB, FXE, and FC, AB features two hydroxamate groups connected via a citryl backbone, rather than a trihydroxamate or peptide-based scaffold. Prior work has shown that AB can rescue *C. crescentus* growth under iron limitation (20), making it an informative probe for defining the substrate boundaries of the HiuABC system.

To evaluate AB utilization, we grew WT, ΔΔΔ *hiuA*$^+$, and ΔΔΔΔ strains in PYE + 300 µM EDTA supplemented with 5 µM AB. As expected, WT growth was strongly enhanced by AB (Fig. S8). In contrast, neither the ΔΔΔ *hiuA*$^+$ strain nor the ΔΔΔΔ strain exhibited any growth enhancement, indicating that HiuA is not required for (and thus does not

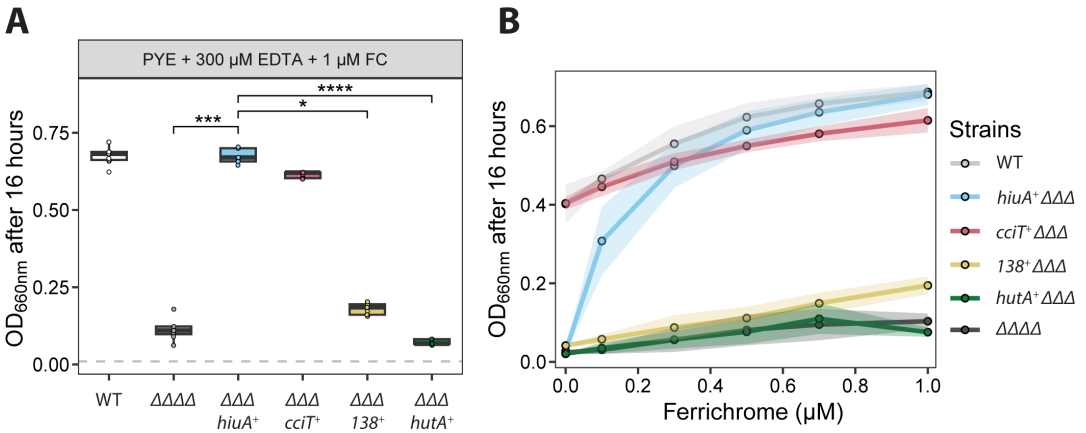



**FIG 5** HiuA is the primary outer membrane importer of FC in *C. crescentus*. (A) Optical densities ($OD_{660}$) of strains after 16 h of growth in PYE broth treated with 300 µM EDTA and supplemented with 1 µM FC. Strains include WT, a strain lacking all four Fur-regulated TBDTs (ΔΔΔΔ), and strains encoding only one of each of the four Fur-regulated TBDTs (*cciT*, *CCNA_00138*, *hutA*, *or hiuA*) while lacking the other three (ΔΔΔ). Cultures were inoculated at $OD_{660}$ = 0.01 (dashed gray line). Box plots display the median and interquartile range (25th–75th percentiles), overlaid with individual data points from independent cultures ($n = 9$). Statistical comparisons of $OD_{660}$ values were performed using a Kruskal-Wallis test followed by Dunn's multiple comparisons test. Significance levels are denoted as follows: $P < 0.05$ (*), $P < 0.001$ (***), and $P < 0.0001$ (****). (B) Optical densities ($OD_{660}$) of strains after 16 h of growth in PYE broth treated with 300 µM EDTA and supplemented with an increasing concentration of FC. Each point represents the mean of nine independent replicates; shading indicates one standard deviation.

mediate) AB uptake, despite its clear role in transporting other hydroxamate-family siderophores. As AB is imported via an HiuA-independent mechanism, we next tested whether the inner membrane components HiuB or HiuC might nevertheless be required for iron extraction from AB once in the periplasm. Growth of Δ*hiuB* and Δ*hiuC* strains was identical to WT under the same EDTA + AB conditions (Fig. S8), demonstrating that neither HiuB nor HiuC is necessary for AB-dependent growth.

Together, these results show that the HiuABC system is dispensable for AB utilization. Moreover, the inability of ΔΔΔ *hiuA*$^+$ and ΔΔΔΔ strains to benefit from AB demonstrates that, although HiuA transports several hydroxamate siderophores with high affinity, it has specificity for specific hydroxamate siderophore structures.

## DISCUSSION

Siderophore-mediated iron acquisition is a widespread bacterial strategy for overcoming iron limitation in aerobic environments (38). In diderms, this process requires energy-dependent transport across the outer membrane via TBDTs, which specifically bind siderophores within defined structural classes (8). Once in the periplasm, ferri-siderophores can be transported to the cytoplasm by inner membrane transporters or reduced to liberate ferrous iron for subsequent import across the inner membrane. *C. crescentus* does not have apparent siderophore biosynthesis genes but encodes 62 predicted TBDTs, several of which are transcriptionally regulated by the ferric uptake repressor (Fur) (20, 22, 39). This suggests a growth/survival strategy centered on scavenging xenosiderophores produced by neighboring organisms in the environment.

We have discovered that the Fur-regulated (40) *hiuABC* operon, comprising three broadly co-conserved genes (Fig. S3), encodes proteins that collectively support the utilization of multiple hydroxamate siderophores. HiuA, a TonB-dependent receptor related to *E. coli* FhuA (20), serves as the primary outer membrane importer for FXB, FXE, and FC but not for the structurally distinct hydroxamate, AB. The inner membrane proteins HiuB (a PepSY–PiuB superfamily member) and HiuC (a small, previously uncharacterized membrane protein) are both required for FXB and FXE utilization, irrespective of the outer membrane entry route. In contrast, FC utilization has distinct genetic requirements: *hiuB* is necessary to utilize FC while *hiuC* is not, indicating a substrate-specific role for HiuC in ferri-siderophore processing. Collectively, these results show that the HiuABC system supports the acquisition of a subset of hydroxamate-family siderophores.

Structural modeling with AlphaFold3 (41) predicts a high-confidence interaction (ipTM = 0.90) between HiuB and HiuC in the inner membrane (Fig. 6A), supporting the hypothesis that these proteins function together as a complex. HiuB contains PepSY domains, which have been associated with periplasmic reductase activity in other systems (42). If the HiuB-HiuC complex catalyzes siderophore iron reduction in the periplasm, this would explain the requirement of both genes for utilization of ferrioxamine siderophores. Supporting this hypothesis, AlphaFold3 modeling of HiuB reveals two putative histidine-ligated heme-binding sites within its transmembrane domain (Fig. 6A and B). These correspond to experimentally resolved heme ligation sites in the structure of the *Pseudomonas aeruginosa* ferrioxamine reductase FoxB, which are proposed to mediate electron transfer to ferrioxamine via a through-space tunneling mechanism (33). We propose that HiuC modulates the reductase activity of HiuB, potentially by influencing substrate specificity. This model aligns with our observation that *hiuC* is required for utilization of ferrioxamines (FXB and FXE) but dispensable for FC utilization, suggesting substrate-dependent regulation of HiuB activity by HiuC.

The *hiuABC* system appears to be mechanistically distinct from the well-studied *fhu* FC uptake system in *E. coli* (32, 43). In the *fhu* system, the outer membrane TBDT (FhuA) is functionally linked to a periplasmic binding protein (FhuD) and an inner membrane ABC transporter (FhuB-FhuC). In contrast, the *hiuABC* operon lacks ABC transporter components; the route of iron or ferri-siderophore transport across the inner membrane remains unknown. It seems likely that HiuB (and in some cases an HiuB-HiuC

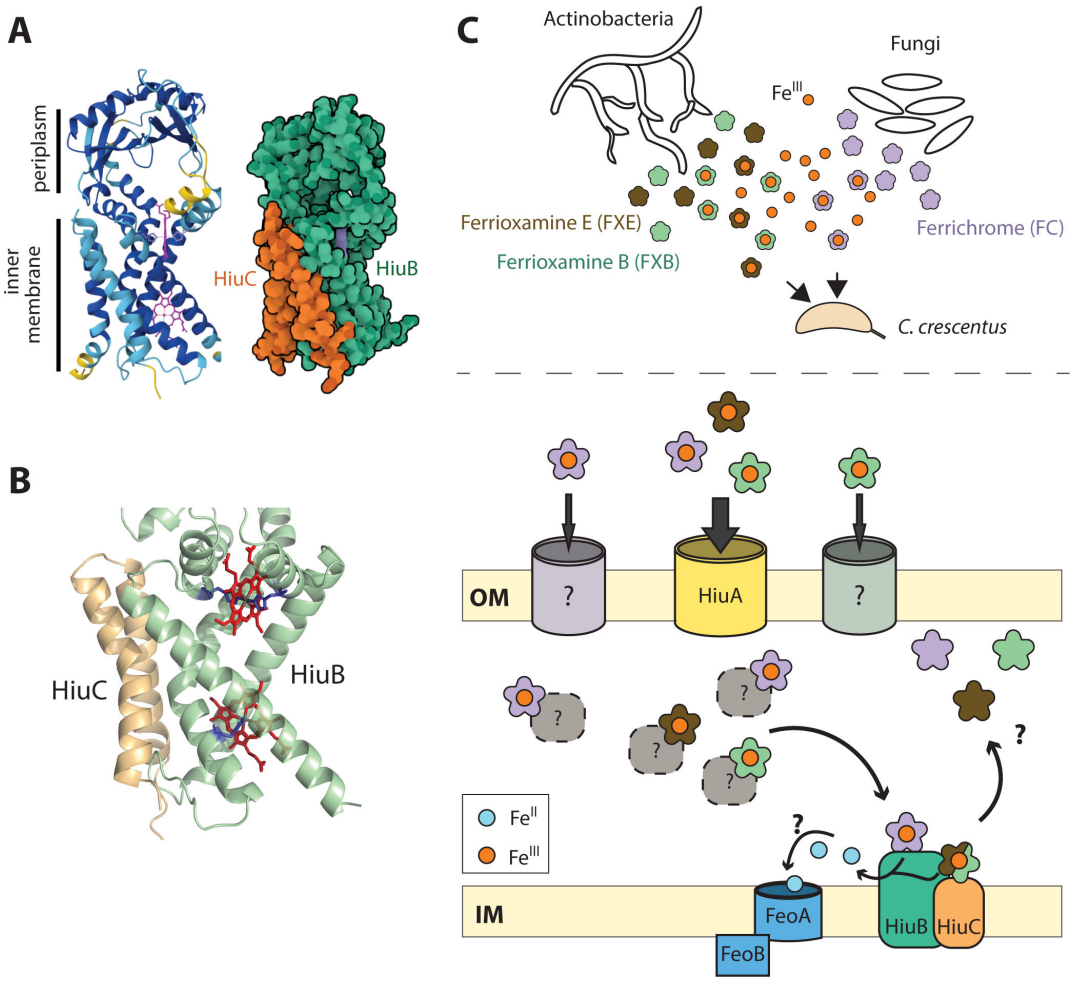



**FIG 6** HiuABC-dependent utilization of hydroxamate siderophores in *C. crescentus*. (A) *Left*: Ribbon diagram structural model of the predicted HiuB:HiuC complex with inner membrane and periplasmic domains labeled. Ribbon cartoon is colored by Alphafold3 pLDDT prediction confidence score from yellow (low) to dark blue (high). Two heme cofactors are shown in purple (ipTM=0.90; pTM=0.88). *Right*: Space-filling model of the predicted HiuB:HiuC complex in the same orientation as left. HiuB is shown in green; HiuC is shown in orange. (B) Zoomed-in view of the transmembrane region of proteins HiuB (green) and HiuC (yellow) showing the predicted heme (red) binding sites. The conserved histidine residues that ligate the heme iron center, as in PDB:7ABW, are shown in dark blue. The lower heme cofactor has only one predicted histidine ligation site, while the upper heme cofactor has two. The bound heme cofactors in HiuB are shown in red. (C) Top: Schematic of siderophore production by bacteria and fungi that commonly occupy the same environment(s) as *Caulobacter* spp. Bottom: Schematic model of ferri-siderophore uptake showing periplasmic Fe(III) reduction mediated by the HiuABC system in *C. crescentus*. At the outer membrane (OM), HiuA mediates high-affinity import of FXB, FXE, and FC. There is evidence that FC also enters through a route independent of the Fur-regulated TBDTs (*huiA*, *cciT*, *hutA*, and *CCNA_00138*). In the periplasm, imported siderophores may be bound by yet-to-be-identified periplasmic binding proteins (dotted line-gray circles). At the inner membrane (IM), HiuB (a PepSY-family protein) and HiuC (a small IM protein) are required for FXB and FXE utilization, possibly by facilitating reductive iron release from the siderophore. In contrast, FC utilization requires HiuB, but not HiuC. The FeoAB system is proposed to mediate the import of ferrous iron (Fe[II]) into the cytoplasm following reduction.

complex) promotes reductive release of hydroxamate-bound iron in the periplasm, thereby facilitating transfer of ferrous iron to an as-yet-unidentified transporter. The FeoAB ABC transport system (44) is a possible candidate for this ferrous iron transport role (Fig. 6C).

The data presented here support the existence of low-affinity, HiuA-independent uptake routes for FXB and FC. This functional redundancy aligns with the expansive repertoire of TBDTs in *C. crescentus* and is consistent with results from other bacteria, where select substrates can be transported by multiple TBDTs (8, 45). Notably, HiuA was the only Fur-regulated TBDT tested that enabled utilization of FC at environmentally relevant concentrations (100 nM), consistent with its role as the primary (and

likely physiological) transporter of this hydroxamate siderophore under iron-limiting conditions typical of soil and aquatic environments. Ferrioxamines and FC are produced by diverse microbes and are commonly found in terrestrial and aquatic ecosystems (6, 7, 46). The ability of *C. crescentus* to utilize these hydroxamates via the *hiuABC* system is expected to enhance its fitness in such iron-scarce habitats. The conserved gene synteny of *hiuABC* across diverse bacterial phyla, including Proteobacteria and Bacteroidota (Fig. S3), suggests that this operon functions broadly as a ferri-hydroxamate utilization module in many genera.

Our results raise the interesting question of how iron acquisition may interface with the *C. crescentus* cell cycle. Nutrient and energy availability are tightly integrated with core cell cycle processes (47–53), and different nutrient restrictions can elicit distinct cell cycle phenotypes (54). In previous work, mutants with diminished intracellular iron levels were found to produce significantly smaller cells than WT (24), consistent with iron limitation constraining biomass accumulation. In the present study, we did not observe overt morphological defects in *hiuABC* mutants or an obvious enrichment for swarmer-, stalked-, or predivisional-cell morphologies under our iron-limiting conditions. However, we have not yet conducted rigorous, quantitative cell-cycle analyses to test whether iron limitation or loss of *hiuABC* function alters the distribution of cell types. Because iron uptake influences cellular growth, we anticipate that perturbations of *hiuABC* and other iron acquisition systems will impact the timing of cell-cycle transitions, particularly under more severe or spatially structured iron limitation. Testing how iron acquisition pathways may influence *C. crescentus* cell-cycle control is an important direction for future work.

The broth-based, genome-wide screening approach reported here enables direct linkage of specific TBDTs to their ferri-siderophore substrates. In the future, this scalable, quantitative platform can facilitate the identification and characterization of other iron acquisition systems. Creation of a barcoded *C. crescentus* library in a background lacking the major (and somewhat promiscuous) *cciO–cciT* iron import system (24) could improve the dynamic range of this screening approach and reveal TBDT-ferri-siderophore pairs that provide only a weak growth advantage in the presence of a competing iron acquisition system. Beyond siderophores, and as shown previously (55), this approach can be adapted to investigate uptake of other metals or organic nutrients in defined or natural media (27), providing new insights into bacterial strategies for nutrient acquisition across ecosystems.

## MATERIALS AND METHODS

### Growth conditions and strain construction

*C. crescentus* CB15 and derived strains were grown at 30°C in PYE medium (0.2% [wt/vol] peptone [Fisher Bioreagents, Lot No. 225155], 0.1% [wt/vol] yeast extract [Fisher Bioreagents, Lot No. 220635], 1 mM $MgSO_4$ [Fisher Chemical, Lot No. 183674], and 0.5 mM $CaCl_2$ [Fisher Chemical, Lot No. 117031]) and is best described as a complex medium. The Fe•EDTA chelate (Sigma-Aldrich, F0518, Lot No. RNBD1641) used to supplement PYE is a 1:1 molar mix of $FeSO_4$ and EDTA (ferrous sulfate chelate solution kept at 4°C, Sigma-Aldrich, F0518). When Fe(III) was used, a 100 mM $FeCl_3$ aqueous stock (pH ~3.0) kept at −20°C was thawed and used to make a working 10 mM stock that was used to generate the ferri-siderophores by mixing 1:1 molar ratio to reach the final concentrations indicated. When an apo- or iron-bound siderophore (desferrichrome/FC [*Ustilago sphaerogena*; Sigma-Aldrich], desferrioxamine B/FXB, FXE [*Streptomyces antibioticus*, Millipore], or AB [TargetMol]) was added to liquid media, it was added to sterile media just before bacterial inoculation. The water used for the preparation of all media was ultra-purified using a Barnsted GenPure water purification system (ThermoFisher). *E. coli* strains were grown at 37°C in LB medium (1% [wt/vol] tryptone, 0.5% [wt/vol] yeast extract, and 1% [wt/vol] NaCl). Growth media were solidified by the addition of 1.5% (wt/vol) agar when necessary. To grow any strain lacking *cciT* on a PYE solid medium, the medium was supplemented with 10 µM Fe•EDTA (Sigma-Aldrich, F0518). Antibiotics

were used at the following concentrations in liquid and solid media, respectively, as appropriate: *C. crescentus*, 5 µg/mL or 25 µg/mL kanamycin, 1 µg/mL or 2 µg/mL chloramphenicol, 1 µg/mL or 2 µg/mL tetracycline, and 20 µg/mL nalidixic acid; *E. coli*, 50 µg/mL kanamycin, 20 µg/mL chloramphenicol, and 10 µg/mL tetracycline. Standard molecular biology techniques were used to construct all plasmids. Detailed information on strains, plasmids, and primers can be found in Table S2. To create plasmids for in-frame deletion allele replacements, the regions flanking the target gene were cloned into pNPTS138 (13). For the generation of fluorescent transcriptional reporter plasmids, promoter regions (200–500 bp upstream of the open reading frame) were cloned into the vector pPTM056 (35). For ectopic expression of individual genes, the entire coding sequences plus stop codon (with their respective promoter regions) were cloned into pMT585 (pXGFPC2) (13), which integrates at the *xylX* locus. In the case of *hiuB* and *hiuC*, the genes were amplified and stitched together with the *hiuABC* operonic promoter before being cloned into pMT585 (13, 32). Ectopic expression of the operon was achieved by amplifying and cloning the entire coding sequence and promoter into a mini-TN7 cassette in pUC18-mTn7K. The cassette was then integrated at the glmS locus using a helper plasmid, pTNS3, encoding the TN7 transposase. For inducible constructs, inserts were cloned into pPTM057 that integrates at the xylose locus and contains a cumate-inducible promoter ($P_{Q5}$) (13, 35). All *C. crescentus* strains harboring pPTM057 were grown in media with 50 µM cumate. All plasmids were introduced into *C. crescentus* by conjugation. For allele replacements, a double recombination strategy was used to select merodiploid strains harboring each pNPTS-based plasmid with kanamycin resistance, followed by *sacB* counter selection on PYE plates containing 3% (wt/vol) sucrose. PCR was used to evaluate colonies that were sucrose resistant and kanamycin sensitive to identify those colonies harboring the null allele. For the construction of strains with multiple TBDT gene deletions, counterselection was performed on PYE sucrose plates supplemented with 10 µM Fe•EDTA (Sigma-Aldrich, F0518).

## Tn-himar-seq to assess genes that support growth enhancement by FXB in the presence of EDTA

An aliquot of a *C. crescentus* CB15 barcoded Tn-himar mutant library (27, 28, 56) was grown in 5 mL of liquid PYE medium containing 5 µg/mL kanamycin for 8 h. One milliliter of this starter culture was set aside as a reference, and for each condition (PYE, PYE with 300 µM EDTA, and PYE with 300 µM EDTA and 1 µM FXB), four replicate 2 mL cultures were inoculated to a starting optical density at 660 nm ($OD_{660}$) of 0.01. Cultures were grown in 100 × 14 mm glass tubes, shaking at 200 RPM at 30°C. After 16 h, cultures were diluted back to an $OD_{660}$ of 0.01 and incubated in the same conditions for an additional 16 h for a total of 32 h of growth. After incubation, 1 mL of each culture was collected by centrifugation at 16,000 × *g* for 3 min. The supernatants were discarded, and the resulting cell pellets were resuspended in 10–20 µL of water and stored at −20°C.

Barcode abundances were determined following the workflow developed by Wetmore et al. (26). Briefly, barcodes were amplified using Q5 polymerase (New England Biolabs) in a 20 µL reaction containing Q5 reaction buffer, GC enhancer, 0.8 units Q5 polymerase, 0.2 mM dNTPs, 0.5 µM of each primer, and 1 µL of the cell suspension, using the following amplification conditions: 98°C for 4 min; 25 cycles of 98°C for 30 s, 55°C for 30 s, and 72°C for 30 s; 72°C for 5 min; followed by a hold at 4°C. The primer set consisted of a universal forward primer, Barseq_P1, and a uniquely indexed reverse primer, Barseq_P2_ITxxx, with the index number denoted by xxx (26). The barcode amplification products were pooled and sequenced as 50 bp single-end reads on an Illumina NovaSeq instrument, using Illumina TruSeq primers. Barcode sequence analysis was carried out using the fitness calculation protocol of Wetmore et al. (26). Barcodes from each sample were counted and compiled using MultiCodes.pl and combineBarSeq.pl scripts. A barcode table was generated, from which the FEBA.R script was used to

calculate fitness score relative to the reference starter culture. Scripts were provided by Morgan Price and are available at https://bitbucket.org/berkeleylab/feba/src/master/.

### Growth measurements

A single colony from a strain grown on a PYE plate was inoculated into 2 mL of liquid PYE medium and grown overnight. The next day, the cultures were diluted to an $OD_{660}$ of 0.15 and outgrown for 2 h before being used to inoculate fresh cultures in the desired experimental condition (medium) at an $OD_{660}$ of 0.01. Cultures were then incubated at 30°C while shaking at 200 rpm. After 16 h of growth, the optical density of the cultures was measured. For extended growth experiments (Fig. 1), optical density was measured at 7, 16, 24, 49, 72, 96, and 121 h.

### Analysis of transcription using fluorescent reporters

Strains harboring fluorescent transcriptional reporter plasmids to monitor the activity of the *feoB cciT*, *hutA*, *or hiuABC* promoters (fused to mNeonGreen) were cultured overnight in triplicate at 30°C in liquid PYE containing 1 µg/mL chloramphenicol. These starter cultures were diluted to an $OD_{660}$ of 0.001 and incubated overnight at 30°C with shaking at 200 rpm. The next morning, these cultures were used to inoculate 500 µL of liquid medium in the wells of a clear 48-well plate. The plate lids were sealed onto the plate body with AeraSeal sealing film (RPI Research Products International) and incubated at 30°C while shaking at 155 RPM. After 2 h, $OD_{660}$ and fluorescence (excitation at 497 ± 10 nm; emission at 523 ± 10 nm) were measured on a Tecan Spark 20M plate reader, and fluorescence values were normalized to the corresponding optical density. Statistical analysis was conducted using R.

## ACKNOWLEDGMENTS

Research reported in this publication was supported in part by the National Institute of General Medical Science award R35GM131762 and by Army Research Office contract W911NF2210105 to S.C.

## AUTHOR AFFILIATION

[1]Department of Microbiology, Genetics, and Immunology, Michigan State University, East Lansing, Michigan, USA

## AUTHOR ORCIDs

Aretha Fiebig http://orcid.org/0000-0002-0612-5029
Sean Crosson http://orcid.org/0000-0002-1727-322X

## FUNDING


| Funder | Grant(s) | Author(s) |
|---|---|---|
| National Institutes of Health | R35GM131762 | Sean Crosson |
| Army Research Office | W911NF2210105 | Sean Crosson |


## AUTHOR CONTRIBUTIONS

Sergio Hernandez-Ortiz, Conceptualization, Data curation, Formal analysis, Investigation, Validation, Visualization, Writing – original draft, Writing – review and editing | Aretha Fiebig, Conceptualization, Formal analysis, Supervision, Visualization, Writing – original draft, Writing – review and editing | Sean Crosson, Conceptualization, Formal analysis, Funding acquisition, Supervision, Visualization, Writing – original draft, Writing – review and editing

## ADDITIONAL FILES

The following material is available online.

### Supplemental Material

**Supplemental figures (JB00400-25-S0001.pdf).** Figures S1 to S8.
**Table S1 (JB00400-25-S0002.xlsx).** RB-TnSeq data.
**Table S2 (JB00400-25-S0003.xlsx).** Strains and plasmids.

## REFERENCES


1. Guerinot ML. 1994. Microbial iron transport. Annu Rev Microbiol 48:743–772. https://doi.org/10.1146/annurev.mi.48.100194.003523
2. Clarke FW, Washington HS. 1924. The composition of the Earth's crust
3. Stumm W, Morgan JJ. 1995. Aquatic chemistry: chemical equilibria and rates in natural waters. 3rd edition. Wiley.
4. LeBlanc AR, Wuest WM. 2024. Siderophores: a case study in translational chemical biology. Biochemistry 63:1877–1891. https://doi.org/10.1021/acs.biochem.4c00276
5. Neilands JB. 1995. Siderophores: structure and function of microbial iron transport compounds. J Biol Chem 270:26723–26726. https://doi.org/10.1074/jbc.270.45.26723
6. Hider RC, Kong X. 2010. Chemistry and biology of siderophores. Nat Prod Rep 27:637–657. https://doi.org/10.1039/b906679a
7. Ahmed E, Holmström SJM. 2014. Siderophores in environmental research: roles and applications. Microb Biotechnol 7:196–208. https://doi.org/10.1111/1751-7915.12117
8. Silale A, van den Berg B. 2023. TonB-dependent transport across the bacterial outer membrane. Annu Rev Microbiol 77:67–88. https://doi.org/10.1146/annurev-micro-032421-111116
9. Kumar A, Yang T, Chakravorty S, Majumdar A, Nairn BL, Six DA, Marcondes Dos Santos N, Price SL, Lawrenz MB, Actis LA, Marques M, Russo TA, Newton SM, Klebba PE. 2022. Fluorescent sensors of siderophores produced by bacterial pathogens. J Biol Chem 298:101651. https://doi.org/10.1016/j.jbc.2022.101651
10. Schalk IJ, Guillon L. 2013. Fate of ferrisiderophores after import across bacterial outer membranes: different iron release strategies are observed in the cytoplasm or periplasm depending on the siderophore pathways. Amino Acids 44:1267–1277. https://doi.org/10.1007/s00726-013-1468-2
11. Hallgren J, Dharamshi JE, Rodríguez-Gijón A, Nuy J, Garcia SL, Jonas K. 2025. Widespread potential for phototrophy and convergent reduction of lifecycle complexity in the dimorphic order *Caulobacterales* . Microbiology. https://doi.org/10.1101/2025.05.26.656076
12. Boutte CC, Srinivasan BS, Flannick JA, Novak AF, Martens AT, Batzoglou S, Viollier PH, Crosson S. 2008. Genetic and computational identification of a conserved bacterial metabolic module. PLoS Genet 4:e1000310. https://doi.org/10.1371/journal.pgen.1000310
13. Thanbichler M, Iniesta AA, Shapiro L. 2007. A comprehensive set of plasmids for vanillate- and xylose-inducible gene expression in *Caulobacter crescentus*. Nucleic Acids Res 35:e137–e137. https://doi.org/10.1093/nar/gkm818
14. Stephens C, Christen B, Fuchs T, Sundaram V, Watanabe K, Jenal U. 2007. Genetic analysis of a novel pathway for D-xylose metabolism in *Caulobacter crescentus*. J Bacteriol 189:2181–2185. https://doi.org/10.1128/JB.01438-06
15. Wilhelm RC, Singh R, Eltis LD, Mohn WW. 2019. Bacterial contributions to delignification and lignocellulose degradation in forest soils with metagenomic and quantitative stable isotope probing. ISME J 13:413–429. https://doi.org/10.1038/s41396-018-0279-6
16. North H, McLaughlin M, Fiebig A, Crosson S. 2023. The *Caulobacter* NtrB-NtrC two-component system bridges nitrogen assimilation and cell development. J Bacteriol 205:e0018123. https://doi.org/10.1128/jb.00181-23
17. Wilhelm RC. 2018. Following the terrestrial tracks of *Caulobacter* - redefining the ecology of a reputed aquatic oligotroph. ISME J 12:3025–3037. https://doi.org/10.1038/s41396-018-0257-z
18. Agler MT, Ruhe J, Kroll S, Morhenn C, Kim ST, Weigel D, Kemen EM. 2016. Microbial hub taxa link host and abiotic factors to plant microbiome variation. PLoS Biol 14:e1002352. https://doi.org/10.1371/journal.pbio.1002352
19. Longley R. 2022. Impact of agricultural management and microbial inoculation on soybean (Glycine max) and its associated microbiome. Michigan State University, East Lansing, Michigan.
20. Balhesteros H, Shipelskiy Y, Long NJ, Majumdar A, Katz BB, Santos NM, Leaden L, Newton SM, Marques MV, Klebba PE. 2017. TonB-dependent heme/hemoglobin utilization by *Caulobacter crescentus* HutA. J Bacteriol 199:e00723-16. https://doi.org/10.1128/JB.00723-16
21. Neugebauer H, Herrmann C, Kammer W, Schwarz G, Nordheim A, Braun V. 2005. ExbBD-dependent transport of maltodextrins through the novel MalA protein across the outer membrane of *Caulobacter crescentus*. J Bacteriol 187:8300–8311. https://doi.org/10.1128/JB.187.24.8300-8311.2005
22. Lohmiller S, Hantke K, Patzer SI, Braun V. 2008. TonB-dependent maltose transport by *Caulobacter crescentus*. Microbiology (Reading) 154:1748–1754. https://doi.org/10.1099/mic.0.2008/017350-0
23. da Silva Neto JF, Lourenço RF, Marques MV. 2013. Global transcriptional response of *Caulobacter crescentus* to iron availability. BMC Genomics 14:549. https://doi.org/10.1186/1471-2164-14-549
24. Hernandez-Ortiz S, Ok K, O'Halloran TV, Fiebig A, Crosson S. 2025. A co-conserved gene pair supports *Caulobacter* iron homeostasis during chelation stress. J Bacteriol 207:e0048424. https://doi.org/10.1128/jb.00484-24
25. Evers A, Hancock RD, Martell AE, Motekaitis RJ. 1989. Metal ion recognition in ligands with negatively charged oxygen donor groups. complexation of iron(III), gallium(III), indium(III), aluminum(III), and other highly charged metal ions. Inorg Chem 28:2189–2195. https://doi.org/10.1021/ic00310a035
26. Wetmore KM, Price MN, Waters RJ, Lamson JS, He J, Hoover CA, Blow MJ, Bristow J, Butland G, Arkin AP, Deutschbauer A. 2015. Rapid quantification of mutant fitness in diverse bacteria by sequencing randomly barcoded transposons. mBio 6:e00306-15. https://doi.org/10.1128/mBio.00306-15
27. Hentchel KL, Reyes Ruiz LM, Curtis PD, Fiebig A, Coleman ML, Crosson S. 2019. Genome-scale fitness profile of *Caulobacter crescentus* grown in natural freshwater. ISME J 13:523–536. https://doi.org/10.1038/s41396-018-0295-6
28. Hershey DM, Fiebig A, Crosson S. 2019. A genome-wide analysis of adhesion in *Caulobacter crescentus* identifies new regulatory and biosynthetic components for holdfast assembly. mBio 10:e02273-18. https://doi.org/10.1128/mBio.02273-18
29. Uchendu CG, Guan Z, Klein EA. 2024. Spatial organization of bacterial sphingolipid synthesis enzymes. J Biol Chem 300:107276. https://doi.org/10.1016/j.jbc.2024.107276
30. Stankeviciute G, Guan Z, Goldfine H, Klein EA. 2019. *Caulobacter crescentus* adapts to phosphate starvation by synthesizing anionic glycoglycerolipids and a novel glycosphingolipid. mBio 10:e00107-19. https://doi.org/10.1128/mBio.00107-19
31. Zik JJ, Yoon SH, Guan Z, Stankeviciute Skidmore G, Gudoor RR, Davies KM, Deutschbauer AM, Goodlett DR, Klein EA, Ryan KR. 2022. *Caulobacter* lipid A is conditionally dispensable in the absence of fur and in the presence of anionic sphingolipids. Cell Rep 39:110888. https://doi.org/10.1016/j.celrep.2022.110888
32. Fecker L, Braun V. 1983. Cloning and expression of the fhu genes involved in iron(III)-hydroxamate uptake by *Escherichia coli*. J Bacteriol 156:1301–1314. https://doi.org/10.1128/jb.156.3.1301-1314.1983
33. Josts I, Veith K, Normant V, Schalk IJ, Tidow H. 2021. Structural insights into a novel family of integral membrane siderophore reductases. Proc Natl Acad Sci USA 118:e2101952118. https://doi.org/10.1073/pnas.2101952118

34. Bharmal M-H, Aretakis JR, Schrader JM. 2020. An improved *Caulobacter crescentus* operon annotation based on transcriptome data. Microbiol Resour Announc 9:01025–20. https://doi.org/10.1128/MRA.01025-20
35. McLaughlin M, Hershey DM, Reyes Ruiz LM, Fiebig A, Crosson S. 2022. A cryptic transcription factor regulates *Caulobacter adhesin* development. PLoS Genet 18:e1010481. https://doi.org/10.1371/journal.pgen.1010481
36. Zhou B, Schrader JM, Kalogeraki VS, Abeliuk E, Dinh CB, Pham JQ, Cui ZZ, Dill DL, McAdams HH, Shapiro L. 2015. The global regulatory architecture of transcription during the caulobacter cell cycle. PLoS Genet 11:e1004831. https://doi.org/10.1371/journal.pgen.1004831
37. Aretakis JR, Gega A, Schrader JM. 2019. Absolute measurements of mRNA translation in *Caulobacter crescentus* reveal important fitness costs of Vitamin B $_{12}$ scavenging . mSystems 4:mSystems https://doi.org/10.1128/mSystems.00170-19
38. Andrews SC, Robinson AK, Rodríguez-Quiñones F. 2003. Bacterial iron homeostasis. FEMS Microbiol Rev 27:215–237. https://doi.org/10.1016/S0168-6445(03)00055-X
39. Marks ME, Castro-Rojas CM, Teiling C, Du L, Kapatral V, Walunas TL, Crosson S. 2010. The genetic basis of laboratory adaptation in *Caulobacter crescentus*. J Bacteriol 192:3678–3688. https://doi.org/10.1128/JB.00255-10
40. da Silva Neto JF, Braz VS, Italiani VCS, Marques MV. 2009. Fur controls iron homeostasis and oxidative stress defense in the oligotrophic alphaproteobacterium *Caulobacter crescentus*. Nucleic Acids Res 37:4812–4825. https://doi.org/10.1093/nar/gkp509
41. Abramson J, Adler J, Dunger J, Evans R, Green T, Pritzel A, Ronneberger O, Willmore L, Ballard AJ, Bambrick J, et al. 2024. Accurate structure prediction of biomolecular interactions with AlphaFold 3. Nature 630:493–500. https://doi.org/10.1038/s41586-024-07487-w
42. Méheust R, Huang S, Rivera-Lugo R, Banfield JF, Light SH. 2021. Post-translational flavinylation is associated with diverse extracytosolic redox functionalities throughout bacterial life. elife 10:e66878. https://doi.org/10.7554/eLife.66878
43. Mademidis A, Köster W. 1998. Transport activity of FhuA, FhuC, FhuD, and FhuB derivatives in a system free of polar effects, and stoichiometry of components involved in ferrichrome uptake. Mol Gen Genet 258:156–165. https://doi.org/10.1007/s004380050718
44. Lau CKY, Krewulak KD, Vogel HJ. 2016. Bacterial ferrous iron transport: the Feo system. FEMS Microbiol Rev 40:273–298. https://doi.org/10.1093/femsre/fuv049
45. Noinaj N, Guillier M, Barnard TJ, Buchanan SK. 2010. TonB-dependent transporters: regulation, structure, and function. Annu Rev Microbiol 64:43–60. https://doi.org/10.1146/annurev.micro.112408.134247
46. Velasquez IB, Ibisanmi E, Maas EW, Boyd PW, Nodder S, Sander SG. 2016. Ferrioxamine siderophores detected amongst iron binding ligands produced during the remineralization of marine particles. Front Mar Sci 3. https://doi.org/10.3389/fmars.2016.00172
47. Beaufay F, Coppine J, Hallez R. 2021. When the metabolism meets the cell cycle in bacteria. Curr Opin Microbiol 60:104–113. https://doi.org/10.1016/j.mib.2021.02.006
48. England JC, Perchuk BS, Laub MT, Gober JW. 2010. Global regulation of gene expression and cell differentiation in *Caulobacter crescentus* in response to nutrient availability. J Bacteriol 192:819–833. https://doi.org/10.1128/JB.01240-09
49. Hallgren J, Jonas K. 2024. Nutritional control of bacterial DNA replication. Curr Opin Microbiol 77:102403. https://doi.org/10.1016/j.mib.2023.102403
50. Ronneau S, Petit K, De Bolle X, Hallez R. 2016. Phosphotransferase-dependent accumulation of (p)ppGpp in response to glutamine deprivation in *Caulobacter crescentus*. Nat Commun 7:11423. https://doi.org/10.1038/ncomms11423
51. Hellenbrand CN, Stevenson DM, Gromek KA, Amador-Noguez D, Hershey DM. 2025. A deoxynucleoside triphosphate triphosphohydrolase promotes cell cycle progression in *Caulobacter crescentus* J Bacteriol 207:e0014525. https://doi.org/10.1128/jb.00145-25
52. North H, Hydorn M, Dworkin J, Fiebig A, Crosson S. 2025. Disrupting NtrC function reveals unexpected robustness in a central cell cycle regulatory network. mBio 16:e0196225. https://doi.org/10.1128/mbio.01962-25
53. SurbhiSShau AK, Chacko FM, Radhakrishnan SK. 2025. A starvation-triggered AAA+ ATPase halts chromosome replication progression by disassembling the bacterial DNA sliding clamp. Curr Biol 35:5264–5277. https://doi.org/10.1016/j.cub.2025.09.042
54. Hallgren J, Koonce K, Felletti M, Mortier J, Turco E, Jonas K. 2023. Phosphate starvation decouples cell differentiation from DNA replication control in the dimorphic bacterium *Caulobacter crescentus*. PLoS Genet 19:e1010882. https://doi.org/10.1371/journal.pgen.1010882
55. Price MN, Wetmore KM, Waters RJ, Callaghan M, Ray J, Liu H, Kuehl JV, Melnyk RA, Lamson JS, Suh Y, Carlson HK, Esquivel Z, Sadeeshkumar H, Chakraborty R, Zane GM, Rubin BE, Wall JD, Visel A, Bristow J, Blow MJ, Arkin AP, Deutschbauer AM. 2018. Mutant phenotypes for thousands of bacterial genes of unknown function. Nature 557:503–509. https://doi.org/10.1038/s41586-018-0124-0
56. Hershey DM, Fiebig A, Crosson S. 2021. Flagellar perturbations activate adhesion through two distinct pathways in *Caulobacter crescentus* mBio 12:e03266-20. https://doi.org/10.1128/mBio.03266-20